analytical chemistry

Article

pubs.acs.org/ac

Simultaneous Separation and Washing of Nonmagnetic Particles in an Inertial Ferrofluid/Water Coflow

Qi Chen,[†,‡] Di Li,[†] Jianhan Lin,[‡] Maohua Wang,[‡] and Xiangchun Xuan*[,†]

[†]Department of Mechanical Engineering, Clemson University, Clemson, South Carolina 29634-0921, United States

[‡]MOA Key Laboratory of Agricultural Information Acquisition Technology (Beijing), China Agricultural University, Beijing 10083, China

Supporting Information

ABSTRACT: Magnetic fluids (e.g., paramagnetic solutions and ferrofluids) have been increasingly used for label-free separation of nonmagnetic particles in microfluidic devices. Their biocompatibility, however, becomes a concern in high-throughput or large-volume applications. One way to potentially resolve this issue is resuspending the particles that are separated in a magnetic fluid immediately into a biocompatible buffer. We demonstrate herein the proof-of-principle of the first integration of negative magnetophoresis and inertial focusing for a simultaneous separation and washing of nonmagnetic particles in coflowing ferrofluid and water streams. The two operations take place in parallel in a simple T-shaped rectangular microchannel with a nearby permanent magnet. We find that the larger and smaller particles' exiting positions (and hence their separation distance) in the sheath water and ferrofluid suspension, respectively, vary with the total flow rate or the flow rate ratio between the two streams.

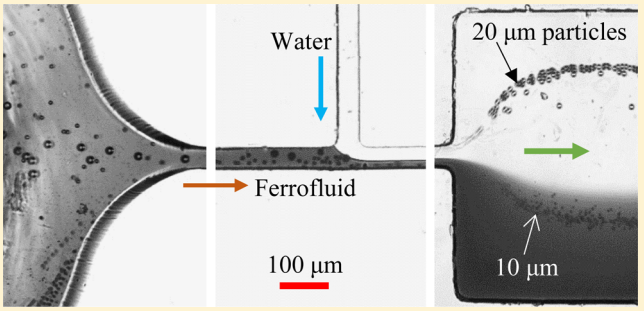

Separating particles (either biological or synthetic) from a mixture in a continuous flow is critical to many lab-on-a-chip applications.[1−3] Magnetic separation[4,5] has several advantages over other active field (e.g., acoustic,[6] electric,[7] and optical[8])-induced particle separation techniques[9,10] including simplicity, low cost, and free of fluid heating, etc.[11−13] It relies on the difference in the magnetic polarization between the particle and suspending medium in response to a magnetic field, which can be achieved by rendering either of these two phases magnetizable.[14,15] In traditional magnetic separation methods such as magnetic-activated cell sorting (MACS),[16] magnetic or magnetically tagged particles experience *positive* magnetophoresis in a nonuniform magnetic field and migrate toward the source of magnetic field.[17−21] On the contrary, nonmagnetic particles (e.g., all kinds of bioparticles except red blood cells[22] and magnetotactic bacteria[23]) that are suspended in a magnetic fluid undertake *negative* magnetophoresis.[24−26] They are repelled to move away from the source of magnetic field at a size-[27−33] and shape-dependent[34,35] rate, enabling a label-free particle separation. Negative magnetophoretic motion has also been increasingly used in the past decade for various other manipulations of nonmagnetic particles in microfluidic devices[36] such as focusing,[37,38] trapping,[39−41] and coating.[42]

Two types of magnetic fluids have thus far been exclusively involved in nonmagnetic particle separations: paramagnetic solutions (e.g., $MnCl_2$ and $GdCl_3$, etc.)[43] and ferrofluids.[44] They both have been demonstrated to manipulate a variety of biological cells (e.g., plant cells,[45−47] bacteria,[47,48] and mammalian cells[49,50]) without affecting much the cell viability. Their biocompatibility is, however, still a concern, especially significant if the concentration of paramagnetic salts or superparamagnetic nanoparticles needs to be increased for an enhanced throughput or the duration of experimental operations needs to be extended for processing a larger volume of biological samples.[51] One way to potentially resolve this issue is resuspending the particles that are separated in a magnetic fluid into a biocompatible buffer. Such a so-called particle washing or medium exchange process[52] can take place either alongside or immediately after the nonmagnetic particle separation preferably on the same chip. It, however, should be as quick as possible to minimize the cross-contamination between the laminar flows of washing buffer and magnetic fluid that mix with each other through diffusion. A number of microfluidic approaches have thus been developed to use either physical barriers[53] or remotely controlled force fields (e.g., acoustic,[54] electric,[55] magnetic,[56] etc.) to achieve a rapid on-chip particle washing. There have also been a few other approaches that exploit the channel structure-induced streamline alteration (in, for example, deterministic lateral displacement,[57] hydrophoresis,[58] and pinched flow fractionation,[59] etc.) or flow-induced (inertial[60] and/or elastic[61,62]) lift force to exchange the particle suspending medium.

Received: May 1, 2017
Accepted: May 26, 2017
Published: May 26, 2017

DOI: 10.1021/acs.analchem.7b01608
Anal. Chem. 2017, 89, 6915−6920

We develop in this work a high-throughput microfluidic approach to simultaneous separation and washing of nonmagnetic particles in a ferrofluid/water coflow. This approach combines the active magnetic force induced in the ferrofluid and the passive inertial force induced in both the ferrofluid and sheath water to transfer only the larger particles across the ferrofluid−water interface. Compared to the existing particle-washing approaches,[52] our proposed hybrid microfluidic approach has the potential to achieve an enhanced sensitivity and flexibility[10] due to the independent control of the magnetic and inertial forces. The effect of the total flow rate of the sheath water and ferrofluid suspension on the particles' exiting positions is experimentally investigated. Also studied is the effect of the flow rate ratio between the two streams.

METHOD

Experiment. Figure 1 shows a picture of the microchannel used in our experiments, which was fabricated in polydimethylsiloxane (PDMS) using a custom-modified soft lithography method.[63] The T-shaped channel consists of a 2 cm long main branch joined by two 4 mm long side branches. It is uniformly 50 μm wide and 100 μm deep in each branch. At the end of the main branch is a 900 μm-wide, 2 mm-long expansion for enhanced visualization at a reduced particle velocity. A neodymium−iron−boron permanent magnet (B224, 1/8 in. × 1/8 in. × 1/4 in., K&J Magnets, Inc.) was embedded into the PDMS slab. It was positioned 500 μm away from the main branch and 4 mm downstream the T-junction. The magnetization direction of the magnet was set to be perpendicular to the chip.

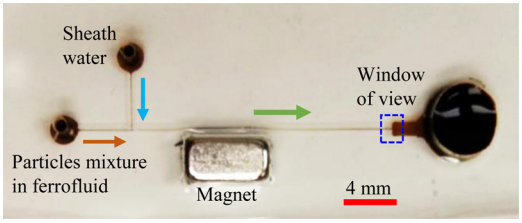

Figure 1. Top-view picture of a T-shaped microchannel (filled with ferrofluid for clarity) with a nearby permanent magnet. The arrows indicate the flow direction in each branch of the channel during the particle separation and washing experiment. The dashed-line box highlights the window of view for particle visualization at the outlet expansion of the channel.

Two types of nonmagnetic polystyrene particles with 10 μm (Thermo Scientific) and 20 μm (Phosphorex Inc.) in diameter were used in the experiment. They were mixed and resuspended in 0.75× EMG 408 ferrofluid that was prepared by diluting the original ferrofluid (1.2% vol. magnetic nanoparticle concentration, Ferrotec Corp.) with deionized water (Fisher Scientific). To prevent particle aggregations and adhesions to channel walls, Tween 20 (0.5% v/v, Fisher Scientific) was added to the particle suspension in ferrofluid. The sheath water and ferrofluid suspension were each driven through one side branch of the T-shaped microchannel (see Figure 1) using an infusion syringe pump (KD Scientific). Particle motion was visualized at the channel's expansion (see the highlighted window of view in Figure 1) and T-junction through an inverted microscope (Nikon Eclipse TE2000U, Nikon Instruments). Digital videos were recorded into a computer with a CCD camera (Nikon DS-Qi1Mc) at a rate of around 15 frames per second. The obtained images were postprocessed using the Nikon imaging software (NIS-Elements AR 2.30).

Mechanism. Figure 2 illustrates the working mechanism of the proposed nonmagnetic particle separation and washing in an inertial ferrofluid/water coflow. The mixture of particles in the ferrofluid is focused by the sheath water to a narrow stream at the T-junction of the microchannel (Figure 2, left panel). They experience a repulsive magnetic force, $\mathbf{F}_M$, in a nonuniform magnetic field and are pushed away from the permanent magnet due to their much smaller magnetization than the suspending ferrofluid,[26,44]

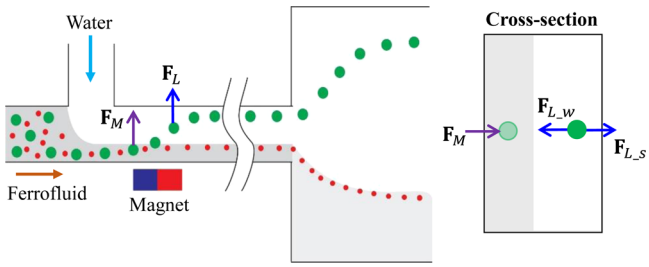

Figure 2. Schematics (not drawn to scale) illustrating the mechanism of nonmagnetic particle separation and washing in an inertial ferrofluid/water coflow. The sheath water prefocuses the particle mixture in the (dark) ferrofluid, where the larger particles experience a greater repulsive magnetic force, $\mathbf{F}_M$, than the smaller ones and can thus reach the ferrofluid/water interface (left panel). The larger particles then migrate to the near-wall equilibrium position in the sheath water due to the action of inertial lift, $\mathbf{F}_L$, that consists of two opposing components: the wall-induced inertial lift, $\mathbf{F}_{L-w}$, and the shear-gradient-induced inertial lift, $\mathbf{F}_{L\_s}$ (right panel).

$$\mathbf{F}_M = -\frac{1}{6}\pi a^3 \mu_0 (\mathbf{M}_f \cdot \nabla)\mathbf{H} \quad (1)$$

$$\mathbf{M}_f = c_0 \mathbf{M}_d [\coth(\alpha) - 1/\alpha] \quad (2)$$

$$\alpha = \frac{\pi d^3 \mu_0 M_d H}{6 k_B T} \quad (3)$$

In the above equations, a is the particle diameter, μ_0 is the permeability of free space, $\mathbf{M}_f$ is the ferrofluid magnetization, $\mathbf{H}$ is the magnetic field vector at the particle center, c_0 is the volume fraction of ferrofluid (superparamagnetic) nanoparticles, $\mathbf{M}_d$ is the saturation moment of ferrofluid nanoparticles of diameter d with M_d being its magnitude, k_B is the Boltzmann constant, and T is the ferrofluid temperature.

Particles also experience a cross-stream lift force in the flow of ferrofluid (and as well water), $\mathbf{F}_L$, whose magnitude, F_L, can be estimated using the following formula,[64]

$$F_L = f_L \rho U_m^2 a^4 / w^2 \quad (4)$$

where f_L is the average lift coefficient that varies from ∼0.02 to 0.05 for channel aspect ratios (width/height) from 0.5 to 2,[65] ρ is the fluid density, U_m is the maximum fluid velocity, and w is the channel width. This passive inertial lift has been theoretically demonstrated to consist of two opposing components (Figure 2, right panel):[66,67] the wall-induced inertial lift, $\mathbf{F}_{L\_w}$, pushes the particles away from the channel walls; the shear-gradient induced inertial lift, $\mathbf{F}_{L\_s}$, directs the particles toward the walls. The balance of these lift components alone leads to two equilibrium positions in our 50 μm wide and

DOI: 10.1021/acs.analchem.7b01608
Anal. Chem. 2017, 89, 6915−6920

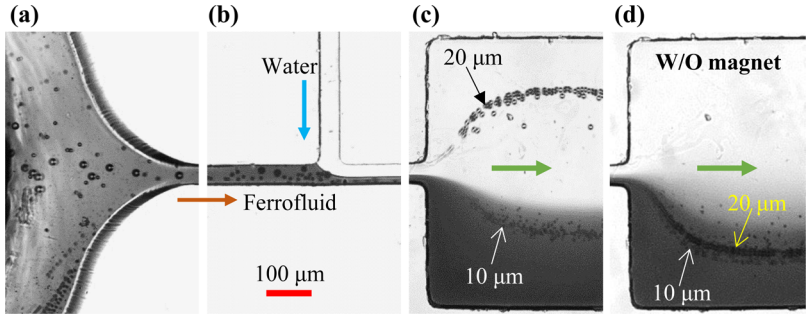

Figure 3. Demonstration of simultaneous washing and separation of 20 μm nonmagnetic particles from 10 μm ones in the inertial flow of 0.75× EMG 408 ferrofluid through a T-shaped microchannel. The flow rates of the ferrofluid-based particle suspension (dark) and sheath water (bright) are 1 mL/h and 3 mL/h, respectively. (a) Snapshot image of randomly distributed particles at the inlet reservoir of the side branch for particle suspension. (b) Snapshot image of sheath water-focused particles at the T-junction (recorded at a reduced flow rate for clarity due to the limited camera speed). (c) Superimposed image of the separated particles in the two fluid streams each at the outlet expansion of the microchannel. (d) Superimposed image of the particle mixture inside the ferrofluid at the outlet expansion when the permanent magnet is removed. The block arrows indicate the flow direction.

100 μm deep microchannel that are each at the center of the longer channel face (i.e., the depth) with a particle-wall distance of around 0.2 times the channel width.[68,69]

The action of the active magnetic force, $\mathbf{F}_M$, alters the equilibrium particle position in inertial focusing by pushing them across the ferrofluid (Figure 2, right panel). As $\mathbf{F}_M$ and $\mathbf{F}_L$ are both strong functions of particle size, we can adjust the flow rate of ferrofluid and/or sheath water such that only the larger particles can reach their interface. Then the passive inertial lift, $\mathbf{F}_L$, takes over and directs the larger particles toward their single equilibrium position inside the water stream as illustrated in Figure 2 (right panel). This simultaneous washing and separation of larger particles from the particle mixture is associated with two dimensionless numbers:[70,71] (1) the (channel) Reynolds number, Re, is the ratio of the inertial force to viscous force,

$$Re = \frac{\rho U D_h}{\eta} = \frac{2\rho Q}{\eta(w + h)} \quad (5)$$

where U is the average fluid velocity and equal to $2U_m/3$ in flows through parallel plates, $D_h = 2wh/(w + h)$ is the hydraulic diameter of rectangular microchannels with h being the height, η is the fluid viscosity, and Q is the volumetric flow rate; (2) the flow rate ratio, α, between the sheath water, Q_w, and the ferrofluid-based particle suspension, Q_f, through the two side branches each, i.e.,

$$\alpha = Q_w/Q_f \quad (6)$$

Note that the definition of Re is based on the total flow rate in the main branch of the microchannel, i.e., $Q = Q_w + Q_f$.

RESULTS AND DISCUSSION

Demonstration of Particle Separation and Washing. Figure 3 shows the top-view images at different locations of the T-shaped microchannel for the simultaneous washing and separation of 20 μm particles from 10 μm particles in 0.75× EMG 408 ferrofluid. The flow rates of the ferrofluid-based particle suspension and sheath water are Q_f = 1 mL/h and Q_w = 3 mL/h in the two side branches with a ratio of α = 3. The flow in the main branch is laminar with Re = 14.7, where the particle Reynolds number, $Re_p = Re(a/D_h)^2$, is on the order of 1 and sufficient for inertial particle focusing.[72] At the inlet of the side branch for the ferrofluid suspension, the two types of particles are mixed and randomly distributed (Figure 3a). They are pinched by the sheath water at the T-junction to flow in a tighter stream along the lower sidewall of the main branch that is closer to the permanent magnet (Figure 3b). The active magnetic force induced in the ferrofluid and the passive inertial lift induced in the ferrofluid and water act together to transfer 20 μm particles from the ferrofluid suspension into the sheath water (Figure 3c). In contrast, 10 μm particles still remain inside the ferrofluid due to the insufficient magnetic force. As the two types of particles exit the microchannel in two distinctly different streams inside the sheath water and ferrofluid, respectively, their separation purity was estimated to be 100%. We did not observe the retention of particles at the T-junction or any other location of the channel. Hence, the particle recovery rate was estimated to be 100% if the impact of particle sedimentation inside the inlet reservoir was neglected. To further confirm the role of magnetic force in this particle separation and washing process, we conducted a control experiment where the permanent magnet was removed while all other conditions were maintained. The two types of particles are both retained within the ferrofluid and still mixed without any visible separation at the outlet expansion of the microchannel (Figure 3d). Moreover, their distance from the lower sidewall in the image (Figure 3d) is smaller than that of 10 μm particles when the magnet is present (Figure 3c) due to the lack of the repulsive magnetic force.

Effect of Flow Rate. Figure 4 shows the flow rate effect on 20 μm particle separation (from 10 μm particles) in 0.75× EMG 408 ferrofluid and washing in the sheath water. The flow rate of the ferrofluid-based particle suspension, Q_f, is varied from 0.1 to 2.2 mL/h while the flow rate ratio between the sheath water and ferrofluid is fixed at α = 3. Therefore, the total flow rate in the main branch of the microchannel varies from 0.4 to 8.8 mL/h, leading to Re increasing from 1.47 to 32.4. At Q_f = 0.1 mL/h, the magnetic force is so strong that 20 μm particles are unable to enter into the main branch and hence absent from the image at the outlet expansion. In contrast, 10 μm particles travel near the interface of the ferrofluid and water streams at the expansion due to the magnetic repulsion in the main branch. They are mildly dispersed because of the insufficient sheath-flow focusing at the T-junction and the weak inertial focusing in the main branch (Re_p = 0.03 for 10 μm particles). At Q_f = 0.2 mL/h, 20 μm particles travel into the main branch in the ferrofluid suspension while leaving it in the sheath water. Their exiting position at the outlet expansion

DOI: 10.1021/acs.analchem.7b01608
Anal. Chem. 2017, 89, 6915−6920

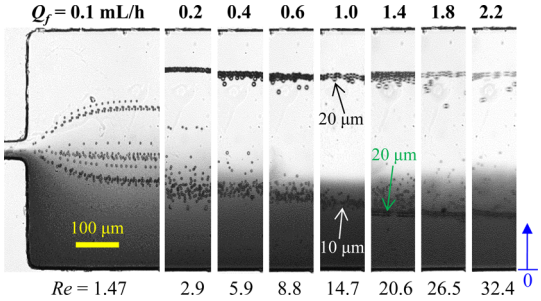

Figure 4. Superimposed images at the outlet expansion of the microchannel illustrating the flow rate effect on the simultaneous washing and separation of 20 μm nonmagnetic particles from 10 μm ones in the inertial flow of 0.75× EMG 408 ferrofluid. The flow rate of the ferrofluid-based particle suspension, Q_f, is varied from 0.1 to 2.2 mL/h (see the labeled values above the images, the resulting values of *Re* are labeled below the images) while the flow rate ratio between sheath water (bright) and ferrofluid suspension (dark) is fixed at $\alpha = 3$. The flow is from left to right in all images. The arrow on the right-most image indicates the reference point to which the particle positions in Figure 5 were measured.

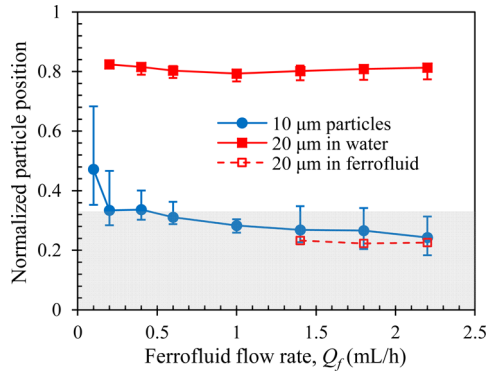

Figure 5. Normalized (by the width of the outlet expansion) exiting positions of 20 and 10 μm particles at the outlet expansion of the microchannel for a range of ferrofluid flow rates. All data points (error bars cover the span of particle stream widths) were obtained from the images in Figure 4. The shaded region (estimated from the images in Figure 4) indicates the area that the ferrofluid suspension approximately occupies at the outlet expansion. The lines are used to guide eyes only.

does not change significantly with the further increase of Q_f, which should be the equilibrium position of inertial focusing in the water side. This is because the required channel length for inertial focusing of 20 μm particles to equilibrium positions[65] (estimated to be only 0.8 cm at Q_f = 0.2 mL/h) is smaller than the length of the downstream main branch after the magnet. In contrast, 10 μm particles still travel near the ferrofluid/water interface but primarily inside the ferrofluid due to the reduced influence of magnetic force at an increasing flow rate. Such a status remains nearly unvaried at Q_f = 0.4 mL/h though the dispersion of 10 μm particles decreases as a result of the increasing inertia.

Increasing the ferrofluid flow rate to Q_f = 0.6 mL/h enables the inertial focusing of 10 μm particles (*Re* = 0.18) to their equilibrium position (the required focusing length[65] was estimated to be about 1 cm). This position in the ferrofluid suspension, however, still remains at near the ferrofluid/water interface due to the action of the repulsive magnetic force. It shifts away from the interface toward the inertial equilibrium position deeper in the ferrofluid at Q_f = 1.0 mL/h and above. Interestingly, part of the 20 μm particles appear at a similar equilibrium position to that of the 10 μm particles inside the ferrofluid for $Q_f \geq$ 1.4 mL/h. This happens due to the reduced residence time for 20 μm particles to experience the magnetic force in the main branch such that not all of them (dispersed in the channel depth direction) can transfer across the ferrofluid/water interface. The variations of the particle exiting positions at the outlet expansion (normalized by its width) with Q_f are shown in Figure 5. Within the entire range of flow rates (or *Re*) under test except for Q_f = 0.1 mL/h, 20 μm particles stay at the inertial equilibrium positions in the sheath water (for Q_f = 1.0 mL/h and below) and as well in the ferrofluid suspension (for Q_f = 1.4 mL/h and above) that are each about 0.2 times the channel width away from the sidewall. In contrast, 10 μm particles remain primarily inside the ferrofluid (see the shaded region in Figure 5) and migrate toward the single inertial equilibrium position therein with the increasing flow rate. The best flow rate for the simultaneous washing and separation of 20 μm particles from 10 μm ones takes place at around Q_f = 1.0 mL/h (see Figure 3c).

We have also studied the separation and washing of 20 μm particles from 10 μm particles in 0.5× EMG 408 ferrofluid. Similar phenomena to those in Figures 5 and 6 for 0.75× EMG

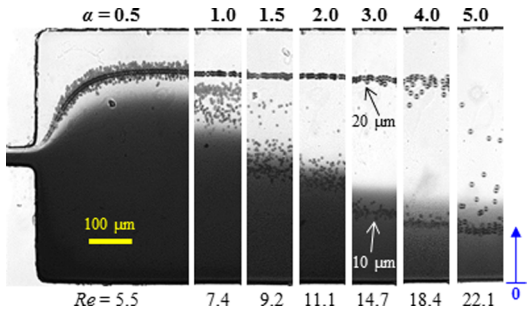

Figure 6. Superimposed images at the outlet expansion of the microchannel illustrating the effect of flow rate ratio, α between the sheath water (bright) and ferrofluid-based particle suspension (dark) on 20 μm particle washing and separation from 10 μm particles. The ferrofluid flow rate is fixed at Q_f = 1.0 mL/h, and $\alpha = Q_w/Q_f$ is varied from 0.5 to 5 (see the labeled values above the images, the resulting values of *Re* are labeled below the images). The flow is from left to right in all images. The arrow on the right-most image indicates the reference point to which the particle positions in Figure 7 were measured.

408 ferrofluid are observed when the flow rate is varied. However, due to the decreased effect of magnetic force, the occurrence of 20 μm particles at the inertial equilibrium position inside the ferrofluid starts under a smaller flow rate in 0.5× ferrofluid (around 0.6 mL/h, see Figures S1 and S2 in Supporting Information) than in 0.75× ferrofluid (1.4 mL/h in Figures 5 and 6). This reduces the flow rate at which the simultaneous particle separation and washing can take place.

Effect of Flow Rate Ratio. Figure 6 shows the effect of flow rate ratio, α, on the washing and separation of 20 and 10 μm particles in 0.75× EMG 408 ferrofluid at a fixed flow rate of Q_f = 1.0 mL/h. The flow rate of the sheath water is varied from 0.5 mL/h (i.e., α = 0.5) to 5 mL/h (i.e., α = 5.0), leading to the increase of *Re* from 5.5 to 22.1. At α = 0.5, both types of particles can transfer across the ferrofluid/water interface due to sufficiently strong negative magnetophoresis (relative to the

DOI: 10.1021/acs.analchem.7b01608
Anal. Chem. 2017, 89, 6915−6920

weak flow) in the ferrofluid suspension. Moreover, they migrate to (coincidentally) similar positions in the sheath water at the outlet expansion, where 20 μm particles are inertially aligned while 10 μm ones are mildly focused. At α = 1.0, the exiting position of 20 μm particles remains nearly unvaried at their inertial equilibrium position in the water stream. In contrast, 10 μm particles, though also exiting the channel inside the water, travel closer to the ferrofluid/water interface in a widened stream due to the insufficient sheath-flow (at the T-junction) and inertial (in the main branch) focusing. Further increasing the flow rate ratio until α = 4.0 does not change visibly the exiting position of 20 μm particles at the outlet expansion. Meanwhile, however, 10 μm particles are no longer able to (completely) cross the ferrofluid/water interface and become less dispersed due to the increasing sheath and inertial focusing effects. Their exiting position at the outlet expansion moves deeper into the ferrofluid stream and shifts toward the inertial equilibrium position therein.

At α = 5.0, 20 μm particles start migrating toward the inertial equilibrium position of 10 μm particles inside the ferrofluid due to the same reason as stated above in Figure 4 (see Q_f = 1.4 mL/h). Moreover, the value of *Re* at which the exiting position of 20 μm particles switches from the sheath water back to the ferrofluid is around 20 in both Figure 6 (for the effect of α) and Figure 4 (for the effect of *Re*). However, there is only one inertial equilibrium position for 20 μm particles in Figure 6, i.e., either within the sheath water for $\alpha \leq$ 4.0 or within the ferrofluid for $\alpha \geq$ 5.0. In contrast, 20 μm particles can have two coexisting equilibrium positions in the water and ferrofluid, respectively, in Figure 4 for $Q_f \geq$ 1.4 mL/h (the high limit was not tested) and α = 3.0. This is probably due to the overfocusing effect from the sheath water at the T-junction when $\alpha \geq$ 5.0, such that the entire particle mixture is prerestricted to the region closely around the inertial equilibrium position inside the ferrofluid.

Figure 7 compares the normalized (by the width of the expansion) exiting positions of the two types of particles (symbols with error bars) at the outlet expansion of the microchannel when the flow rate ratio is varied. The corresponding shift of the location of the ferrofluid/water interface is also included in Figure 7 (dashed line) for better identifying the particle washing effect at varying flow rate ratios. These interfacial positions, which were estimated from the experimental images in Figure 6, are, however, only approximate due to the inherent diffusion between the ferrofluid and sheath water flows. In the range of α = 0.5 to 4.0, the exiting position of 20 μm particles remains almost unchanged at the single inertial equilibrium position inside the sheath water, which is about 0.2 times the channel width away from the upper sidewall. In contrast, 10 μm particles stay within the ferrofluid stream for α = 1.5 and above, whose exiting position becomes increasingly closer to the inertial equilibrium position that is 0.2 times the channel width away from the lower sidewall. The best performance of the simultaneous particle washing and separation is achieved for α = 3.0 to 4.0.

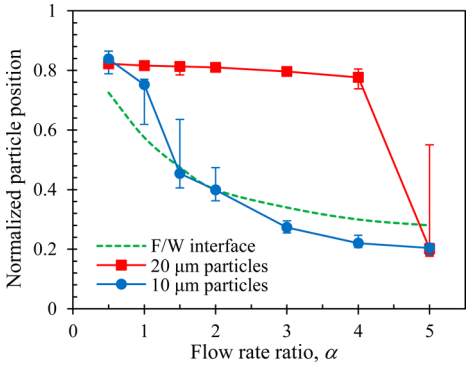

Figure 7. Normalized (by the width of the outlet expansion) exiting positions of 20 and 10 μm particles at the outlet expansion of the microchannel for a range of flow rate ratios. All data points (symbols with error bars to cover the span of particle stream widths) were obtained from the images in Figure 6. The dashed line indicates the approximate location of the ferrofluid and water interface that was estimated directly from the images in Figure 6. The solid lines are used to guide eyes only.

CONCLUSIONS

We have developed a simple microfluidic device for the proof-of-principle study of continuous separation of nonmagnetic particles by size in a ferrofluid flow and simultaneous washing of the separated larger particles in a coflowing sheath water. These two parallel operations are enabled by the active magnetic force induced in the ferrofluid and the passive inertial lift induced in the ferrofluid and water flows. Due to the particle size and flow rate dependences of the force-driven particle magnetophoresis and inertial migration, we can alter the larger and smaller particles' exiting positions in the water and ferrofluid streams by adjusting the total flow rate or the flow rate ratio between the two streams. We recognize that the size of the particles used in our experiments is relatively large compared to that of common cells (e.g., red and white blood cells). To work with smaller cells, we can increase the length and/or reduce the width of the microchannel for enhanced effects of magnetic deflection and inertial focusing. We are currently developing a three-dimensional numerical model to simulate the simultaneous particle separation and washing process in the ferrofluid/water coflow and understand the impact of the ferrofluid/water mixing. We will use this model to study the resolution limit of the proposed technique and understand the determining factors. We will also use the optimized device to demonstrate the separation and washing of biological cells in an inertial ferrofluid/water coflow with an enhanced biocompatibility as compared to the separation alone in a pure ferrofluid flow.

ASSOCIATED CONTENT

Supporting Information

The Supporting Information is available free of charge on the ACS Publications website at DOI: 10.1021/acs.analchem.7b01608.

Experimental results for the simultaneous separation and washing of 20 μm particles from 10 μm particles in the inertial flow of 0.5× EMG 408 ferrofluid (PDF)

AUTHOR INFORMATION

Corresponding Author

*E-mail: xcxuan@clemson.edu. Fax: 864-656-7299.

ORCID

Xiangchun Xuan: 0000-0003-0158-4186

Notes

The authors declare no competing financial interest.

DOI: 10.1021/acs.analchem.7b01608
Anal. Chem. 2017, 89, 6915−6920

■ ACKNOWLEDGMENTS

This work was supported by China Scholarship Council (CSC)-Chinese Government Graduate Student Overseas Study Program (Q. Chen) and NSF under grant CBET-1150670 (X. Xuan).

■ REFERENCES

(1) Pamme, N. *Lab Chip* **2007**, *7*, 1644−1659.
(2) Gossett, D. R.; Weaver, W. M.; Mach, A. J.; Hur, S. C.; Tse, H. T.; Lee, W.; Amini, H.; Di Carlo, D. *Anal. Bioanal. Chem.* **2010**, *397*, 3249−3267.
(3) Karimi, A.; Yazai, S.; Ardekani, A. M. *Biomicrofluidics* **2013**, *7*, 021501.
(4) Pamme, N. *Lab Chip* **2006**, *6*, 24−38.
(5) Hejazian, M.; Li, W. H.; Nguyen, N. T. *Lab Chip* **2015**, *15*, 959−970.
(6) Laurell, T.; Peterson, F.; Nilsson, A. *Chem. Soc. Rev.* **2007**, *36*, 492−506.
(7) Pethig, R. *Biomicrofluidics* **2010**, *4*, 022811.
(8) Kayani, A. A.; Khoshmanesh, K.; Ward, S. A.; Mitchell, A.; Kalantar-zadeh, K. *Biomicrofluidics* **2012**, *6*, 031501.
(9) Sajeesh, P.; Sen, A. K. *Microfluid. Nanofluid.* **2014**, *17*, 1−52.
(10) Yan, S.; Zhang, J.; Yuan, D.; Li, W. *Electrophoresis* **2017**, *38*, 238−249.
(11) Zborowski, M.; Chalmers, J. J. *Anal. Chem.* **2011**, *83*, 8050−8056.
(12) Nguyen, N. T. *Microfluid. Nanofluid.* **2012**, *12*, 1−16.
(13) Yang, R. J.; Hou, H. H.; Wang, Y. N.; Fu, L. M. *Sens. Actuators, B* **2016**, *224*, 1−15.
(14) Suwa, M.; Watarai, H. *Anal. Chim. Acta* **2011**, *690*, 137−147.
(15) Cao, Q.; Han, X.; Li, L. *Lab Chip* **2014**, *14*, 2762−2777.
(16) Miltenyi, S.; Muller, W.; Weichel, W.; Radbruch, A. *Cytometry* **1990**, *11*, 231−238.
(17) Pamme, N.; Manz, A. *Anal. Chem.* **2004**, *76*, 7250−7256.
(18) Inglis, D. W.; Riehn, R.; Sturm, J. C.; Austin, R. H. *J. Appl. Phys.* **2006**, *99*, 08K101.
(19) Kim, J.; Cho, H.; Han, S. I.; Han, K. H. *Anal. Chem.* **2016**, *88*, 4857−4863.
(20) Hoshino, K.; Huang, Y. Y.; Lane, N.; Huebschman, M.; Uhr, J. W.; Frenkel, E. P.; Zhang, X. *Lab Chip* **2011**, *11*, 3449−3457.
(21) Zhou, R.; Wang, C. *Microfluid. Nanofluid.* **2016**, *20*, 1−11.
(22) Zborowski, M.; Ostera, G. R.; Moore, L. R.; Milliron, S.; Chalmers, J. J.; Schechter, A. N. *Biophys. J.* **2003**, *84*, 2638−2645.
(23) Lee, H.; Purdon, A. M.; Chu, V.; Westervelt, R. M. *Nano Lett.* **2004**, *4*, 995−998.
(24) Peyman, S. A.; Kwan, E. Y.; Margarson, O.; Iles, A.; Pamme, N. *J. Chromatogr. A* **2009**, *1216*, 9055−9062.
(25) Zhu, T.; Lichlyter, D. J.; Haidekker, M. A.; Mao, L. *Microfluid. Nanofluid.* **2011**, *10*, 1233−1245.
(26) Liang, L.; Zhu, J.; Xuan, X. *Biomicrofluidics* **2011**, *5*, 034110.
(27) Zhu, T.; Marrero, F.; Mao, L. *Microfluid. Nanofluid.* **2010**, *9*, 1003−1009.
(28) Vojtisek, M.; Tarn, M. D.; Hirota, N.; Pamme, N. *Microfluid. Nanofluid.* **2012**, *13*, 625−635.
(29) Liang, L.; Xuan, X. *Biomicrofluidics* **2012**, *6*, 044106.
(30) Zhou, Y.; Song, L.; Yu, L.; Xuan, X. *J. Magn. Magn. Mater.* **2016**, *412*, 114−122.
(31) Zhou, R.; Wang, C. *Biomicrofluidics* **2016**, *10*, 034101.
(32) Zhang, J.; Yan, S.; Yuan, D.; Zhao, Q.; Tan, S. H.; Nguyen, N. T.; Li, W. *Lab Chip* **2016**, *16*, 3947−3956.
(33) Zhou, Y.; Song, L.; Yu, L.; Xuan, X. *Microfluid. Nanofluid.* **2017**, *21*, 14.
(34) Zhou, Y.; Xuan, X. *Appl. Phys. Lett.* **2016**, *109*, 102405.
(35) Zhou, R.; Bai, F.; Wang, C. *Lab Chip* **2017**, *17*, 401−406.
(36) Zhao, W.; Cheng, R.; Miller, J.; Mao, L. *Adv. Funct. Mater.* **2016**, *26*, 3916−3932.
(37) Zhu, T.; Cheng, R.; Mao, L. *Microfluid. Nanofluid.* **2011**, *11*, 695−701.
(38) Liang, L.; Xuan, X. *Microfluid. Nanofluid.* **2012**, *13*, 637−643.
(39) Tarn, M. D.; Peyman, S. A.; Pamme, N. *RSC Adv.* **2013**, *3*, 7209−7214.
(40) Hejazian, M.; Nguyen, N. T. *Biomicrofluidics* **2016**, *10*, 044103.
(41) Tarn, M. D.; Elders, L. T.; Peyman, S. A.; Pamme, N. *RSC Adv.* **2015**, *5*, 103776−103781.
(42) Winkleman, A.; Perez-Castillejos, R.; Gudiksen, K. L.; Phillips, S. T.; Prentiss, M.; Whitesides, G. M. *Anal. Chem.* **2007**, *79*, 6542−6550.
(43) Shen, F.; Hwang, H.; Hahn, Y. K.; Park, J. K. *Anal. Chem.* **2012**, *84*, 3075−3081.
(44) Rosensweig, R. E. *Annu. Rev. Fluid Mech.* **1987**, *19*, 437−463.
(45) Zeng, J.; Chen, C.; Vedantam, P.; Tzeng, T. R.; Xuan, X. *Microfluid. Nanofluid.* **2013**, *15*, 49−55.
(46) Zeng, J.; Deng, Y.; Vedantam, P.; Tzeng, T. R.; Xuan, X. *J. Magn. Magn. Mater.* **2013**, *346*, 118−123.
(47) Zhu, T.; Cheng, R.; Lee, S. A.; Rajaraman, E.; Eiteman, M. A.; Querec, T. D.; Unger, E. R.; Mao, L. *Microfluid. Nanofluid.* **2012**, *13*, 645−654.
(48) Wang, Z. M.; Wu, R. G.; Wang, Z. P.; Ramanujan, R. V. *Sci. Rep.* **2016**, *6*, 26945.
(49) Winkleman, A.; Gudiksen, K. L.; Ryan, D.; Whitesides, G. M.; Greenfield, D.; Prentiss, M. *Appl. Phys. Lett.* **2004**, *85*, 2411−2413.
(50) Zhao, W.; Zhu, T.; Cheng, R.; Liu, Y.; He, J.; Qiu, H.; Wang, L.; Nagy, T.; Querec, T. D.; Unger, E. R.; Mao, L. *Adv. Funct. Mater.* **2016**, *26*, 3990−3998.
(51) Rodriguez-Villarreal, A. I.; Tarn, M. D.; Madden, L. A.; Lutz, J. B.; Greenman, J.; Samitier, J.; Pamme, N. *Lab Chip* **2011**, *11*, 1240−1248.
(52) Tarn, M. D.; Lopez-Martinez, M. J.; Pamme, N. *Anal. Bioanal. Chem.* **2014**, *406*, 139−161.
(53) Sochol, R. D.; Li, S.; Lee, L. P.; Lin, L. *Lab Chip* **2012**, *12*, 4168−4177.
(54) Petersson, F.; Nilsson, A.; Jonsson, H.; Laurell, T. *Anal. Chem.* **2005**, *77*, 1216−1221.
(55) Tornay, R.; Braschler, T.; Demierre, N.; Steitz, B.; Finka, A.; Hofmann, H.; Hubbell, J. A.; Renaud, P. *Lab Chip* **2008**, *8*, 267−273.
(56) Phurimsak, C.; Tarn, M. D.; Peyman, S. A.; Greenman, J.; Pamme, N. *Anal. Chem.* **2014**, *86*, 10552−10559.
(57) Chen, Y.; D'Silva, J.; Austin, R. H.; Sturm, J. C. *Biomicrofluidics* **2015**, *9*, 054105.
(58) Kim, B.; Lee, J. K.; Choi, S. *BioChip J.* **2016**, *10*, 81−87.
(59) Chiang, Y.; West, J. *Lab Chip* **2013**, *13*, 1031−1034.
(60) Dudani, J. S.; Go, D. E.; Gossett, D. R.; Tan, A. P.; Di Carlo, D. *Anal. Chem.* **2014**, *86*, 1502−1510.
(61) Yuan, D.; Zhang, J.; Yan, S.; Peng, G.; Zhao, Q.; Alici, G.; Du, H.; Li, W. *Electrophoresis* **2016**, *37*, 2147−2155.
(62) Ha, B.; Park, J.; Destgeer, G.; Jung, J. H.; Sung, H. J. *Anal. Chem.* **2016**, *88*, 4205−4210.
(63) Zhu, J.; Liang, L.; Xuan, X. *Microfluid. Nanofluid.* **2012**, *12*, 65−73.
(64) Asmolov, E. S. *J. Fluid Mech.* **1999**, *381*, 63−87.
(65) Di Carlo, D. *Lab Chip* **2009**, *9*, 3038−3046.
(66) Ho, B. P.; Leal, L. G. *J. Fluid Mech.* **1974**, *65*, 365−400.
(67) Martel, J. M.; Toner, M. *Annu. Rev. Biomed. Eng.* **2014**, *16*, 371−396.
(68) Zhang, J.; Yan, S.; Yuan, D.; Alici, G.; Nguyen, N. T.; Warkiani, M. E.; Li, W. *Lab Chip* **2016**, *16*, 10−34.
(69) Asgar, A.; Bhagat, S.; Kuntaegowdanahalli, S. S.; Papautsky, I. *Phys. Fluids* **2008**, *20*, 101702.
(70) Lu, X.; Liu, C.; Hu, G.; Xuan, X. *J. Colloid Interface Sci.* **2017**, *500*, 182−201.
(71) Lu, X.; Xuan, X. *Anal. Chem.* **2015**, *87*, 4560−4565.
(72) Di Carlo, D.; Irimia, D.; Tompkins, R. G.; Toner, M. *Proc. Natl. Acad. Sci. U. S. A.* **2007**, *104*, 18892−18897.

DOI: 10.1021/acs.analchem.7b01608
Anal. Chem. 2017, 89, 6915−6920